

New Insights into Manganese Local Environment in MnS-1 Nanocrystals

Alenka Ristić,[†] Matjaž Mazaj,[†] Iztok Arčon,^{‡,§} Nina Daneu,[§] Nataša Zabukovec Logar,^{†,‡} Roger Gläser,^{||} and Nataša Novak Tušar^{*,†,‡}

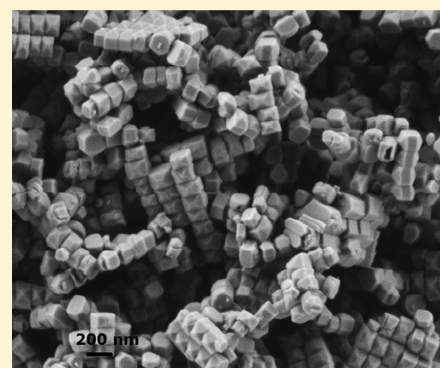
[†]National Institute of Chemistry, Hajdrihova 19, 1000 Ljubljana, Slovenia

[‡]University of Nova Gorica, Vipavska 13, 5000 Nova Gorica, Slovenia

[§]Jožef Stefan Institute, Jamova 1000 Ljubljana, Slovenia

^{||}Institute of Chemical Technology, University of Leipzig, Leipzig, Germany

ABSTRACT: Manganese plays an important role in redox catalysis using zeolites as inorganic support materials, but the formation of the preferred redox manganese species (framework or extraframework) is still not well understood. Herein, the influence of the amount of manganese together with conventional and microwave-assisted hydrothermal synthesis paths on the formation of manganese species within the zeolite silicalite-1 (S-1) with MFI structure was investigated. It was found out that both synthesis procedures led to the formation of framework and extraframework manganese species, but in different molar ratios. However, the conventional synthesis procedure with all Mn/Si molar ratios generates more framework Mn in comparison to the microwave procedure. Additionally, the diminution of the zeolite crystals to nanoscale from 100 to 200 nm was achieved via the conventional procedure for the first time. UV–vis, Raman, and X-ray absorption spectroscopic analyses revealed different local environments of manganese: Mn³⁺ incorporated into the silicalite-1 framework as “framework manganese” and Mn^{2+/3+} present as “extraframework manganese” (Mn₂O₃, Mn₃O₄). TEM reveals the presence of Mn₃O₄ nanorods. Both framework manganese and extraframework manganese exhibit good catalytic activity for styrene epoxidation. Catalytic results suggest that, in oxidation reactions of hydrocarbons, framework manganese is more active at lower Mn contents (Mn/Si < 0.015), whereas extraframework manganese is more active at higher loadings (Mn/Si > 0.015).



INTRODUCTION

Interest in the development of environmentally benign, selective, and stable catalysts for specific purposes has been growing in the last decade. Manganese is one of the most intensively used elements for redox catalysis.¹ In order to obtain recyclable as well as stable catalysts, it is often preferred to isolate and stabilize the redox-active metal species by incorporation into inorganic matrices as framework or/and extraframework species.² Zeolites, i.e., microporous aluminosilicates with pore openings up to 2 nm, are already widely applied as inorganic matrices for stabilization of manganese redox sites in heterogeneously catalyzed conversion.³ However, the optimal synthesis strategy which would lead to the preferred manganese redox species in certain framework types of zeolites remains a matter of debate due to the challenging characterization of the often very low concentration of manganese present (typically below 1 wt %). For example, hydrothermal synthesis and post-synthesis procedures can promote different forms of manganese species, from isolated ions in framework and extraframework positions to single oxides (MnO, Mn₂O₃, and MnO₂) or mixed oxides such as Mn₃O₄ in Mn-containing zeolites.⁴

Silicalite-1 is a high-silica zeolite with an MFI framework topology. Incorporation of manganese into micrometer-sized crystals of this zeolite with sizes of 100–200 μm generates framework manganese redox sites.³ Meng reported a facile synthesis of a Mn-containing MFI-type zeolite by hydrothermal synthesis from a clear solution using a manganese organic precursor and silicates at 180 °C for 2 days, preparing hexagonal platelets with particle sizes of 500–700 nm.⁵ Recently, the incorporation of manganese into silicalite-1 was achieved by the hydrothermal conversion of manganese-exchanged magadiite under neutral conditions (crystals 2–10 μm in size),⁶ while a two-step procedure containing mechanochemical pretreatment and hydrothermal synthesis led to the incorporation of a high content of manganese (up to 6 mol %) into the framework (crystals 10–30 μm in size).⁷

The diminution of the particle size from the micrometer to the nanometer scale results in a larger specific surface area of the catalyst and, thus, a higher activity. Clear solutions with an excess of organic templates (SDAs) are generally used for the

Received: August 6, 2018

Revised: April 11, 2019

Published: May 2, 2019

preparation of zeolite nanoparticles. These systems provide the necessary conditions for uniform nucleation and crystal growth. Consequently, the obtained nanocrystals are uniform in size.⁸ Tetraethyl orthosilicate (TEOS) as a source of silica, the temperature, and the time of crystallization play important roles in the control of size of the obtained silicalite-1 nanocrystals.⁹ To reduce the particle size, different heating technologies can be used: for example, microwave-assisted synthesis, which can provide an efficient control of particle size distribution.^{8,10} In addition to controlling the particle size effect, microwave-assisted synthesis can provide also rapid volumetric heating with a shorter synthesis time and higher synthesis rate, selectivity, and yield in comparison to the conventional hydrothermal preparation method.¹¹ As a result, microwave heating can realize fast crystallization and rapid materials preparation in minutes, while hours or even days are needed by conventional heating methods. Therefore, microwave synthesis can lead to relatively low cost, energy savings, and high efficiency for materials preparation.¹²

Recently, we have prepared a heterogeneous Fenton-type nanocatalyst by incorporation of manganese into silicate nanoparticles of mesostructured KIL-2.¹³ Manganese was incorporated into the silicate framework with a molar Mn/Si ratio of up to 0.01; when the manganese concentration exceeded this value, manganese species were deposited on the surface of the materials as manganese oxide nanoparticles. In addition, in our preliminary synthesis using microwave irradiation, silicalite-1 nanoparticles with Mn₂O₃ species, which were well distributed between silicalite-1 nanoparticles, served as active sites for polysulfide adsorption in lithium sulfur batteries.¹⁴

In this work, the preparation of manganese-containing silicalite-1 nanocrystals by microwave-assisted and conventional hydrothermal synthesis with tunable manganese local environment is presented. Manganese local environments in the resulting materials were determined by UV–vis, Raman, and X-ray absorption (XAS) spectroscopic techniques supported by TEM analysis. The catalytic activity of the materials was tested in styrene epoxidation.

■ EXPERIMENTAL SECTION

Catalyst Preparation. Manganese acetate (99%, Merck) solution, TEOS (98%, Acros), and TPAOH (40%, Alfa Aesar) were mixed at room temperature, respectively. A clear brown solution with molar composition 10 SiO₂:*x* MnO:4 TPAOH:195 H₂O (*x* = 0.05, 0.1, 0.2, 0.5) were aged with stirring for 1 day at room temperature. After aging, 20 mL of the clear solution was transferred into a Teflon-lined stainless steel autoclave for one-step hydrothermal conventional synthesis or into the Teflon autoclave for two-step microwave synthesis in an ETHOS 1600 microwave oven (Milestone). The one-step hydrothermal syntheses were performed at 175 °C for 1 day, while the two-step microwave heating was performed by the following regime: the first step at a temperature of 80 °C for 30 min and the second step at 150 °C for 20 min. After the syntheses, the solid products were separated by rapid centrifugation, washed with distilled water, and dried at 60 °C for several hours. The obtained products were calcined at 500 °C for 5 h in an air flow.

Products obtained via microwave and conventional hydrothermal synthesis were denoted MnS-1-MW and MnS-1-K, respectively. Furthermore, products obtained with different molar ratios were denoted as e.g. 005MnS-1-MW (Mn/Si = 0.005) and 005MnS-1-K (Mn/Si = 0.005).

Catalyst Characterization. The X-ray powder diffraction (XRD) patterns were recorded on a PANalytical X'Pert PRO high-resolution diffractometer with Alpha configuration using Cu K α radiation

(1.5406 Å) in the 2 θ range from 5 to 50° 2 θ using a step of 0.034° and a collection time of 100 s per step on a fully opened X'Celerator detector. Morphology and surface properties were observed by scanning electron microscopy (SEM) on a Zeiss Supra 3VP microscope. Elemental analysis was performed by the EDX method with an INCA Energy system attached to the Zeiss Supra 3VP microscope. The structures of 05MnS-1-MW and 01MnS-1-MW were investigated by high-resolution transmission electron microscopy (HRTEM) on a JEOL JEM 2100 200 kV field-emission gun (FEG) microscope. The sample was dispersed in ethanol and placed on a copper holey carbon grid. The specimen was additionally coated with carbon in order to prevent excessive charging of the samples under the electron beam. UV–vis diffuse reflectance (DR) spectra were recorded on a PerkinElmer Lambda 35 apparatus equipped with a Praying Mantis accessory. Background was recorded with Spectralon reference. Fine powdered samples were scanned in the spectral range between 200 and 1100 nm, with a slit set to 2 nm and a scanning speed of 480 nm/min. Raman spectra were recorded in the spectral range from 70 to 1600 cm⁻¹ using a Witec Alpha 300 confocal microscope that employed a green laser with an excitation wavelength of 532 nm, an accumulation time of 50 s, and a resolution of 4 cm⁻¹ at 10 mW laser power. Mn K-edge X-ray absorption spectra of MnS-1 samples with different amounts of Mn from 0.01 to 0.05 Mn/Si, synthesized via a conventional hydrothermal or microwave procedure, and reference Mn compounds with different Mn valence states and local structure (Mn²⁺O, Mn^{2.7+}₃O₄, Mn³⁺₂O₃, Mn⁴⁺O₂, and Mn³⁺S-1-inc³) were measured in the energy region of the Mn K-edge in transmission mode at the XAFS beamline of the ELETTRA synchrotron facility in Trieste, Italy, and at the P65 beamline of PETRA III at DESY, Hamburg. Both beamlines provided a Si(111) double-crystal monochromator with about 1 eV resolution at the Mn K-edge. The samples were prepared as self-supporting pellets with an absorption thickness (μ d) of about 2.5 above the Mn K-edge, while reference Mn samples were pressed from a homogeneous mixture of the Mn compound and boron nitride powder into self-supporting pellets with a total absorption thickness of about 1.5 above the Mn K-edge. At the XAFS beamline the absorption spectra were measured within the interval -250 to +1000 eV relative to the Mn K-edge. In the XANES region equidistant energy steps of 0.3 eV were used, while for the EXAFS region equidistant *k* steps of 0.03 Å⁻¹ were adopted with an integration time of 1 s/step. At the P65 beamline the absorption spectra were measured in the energy region from -150 eV to +1000 eV relative to the Mn K-edge in continuous fast (3 min) scans and rebinned to the same energy and *k* steps for XANES and EXAFS regions. Four to eight repetitions were collected for each sample and superimposed to improve the signal to noise ratio. Exact energy calibration was established with the simultaneous absorption measurements on Mn metallic foil inserted between the second and third ionization cells. The analysis of XANES and EXAFS spectra was performed with the Demeter (IFEFFIT) program package,¹⁵ in combination with FEFF6 program code¹⁶ for ab initio calculation of photoelectron scattering paths.

The catalytic properties of MnS-1-MW from microwave-assisted hydrothermal synthesis and of MnS-1-K prepared by conventional hydrothermal synthesis were studied in the epoxidation of styrene in a batch reactor in liquid acetonitrile under reflux at 1 bar and 343 K. The catalytic experiments were carried out as described in the literature,¹⁷ except that an overall reaction volume $V_{\text{reaction}} = 20 \text{ cm}^3$ was used.

■ RESULTS AND DISCUSSION

Structural Properties. The method of preparation either using the microwave-assisted hydrothermal (products denoted MnS-1-MW) or the conventional synthesis (products denoted MnS-1-K) with different temperatures and times of crystallization can influence the local environment of the resulting manganese species within the silicalite-1 framework. Before hydrothermal synthesis, a light pink clear solution was prepared by mixing an aqueous manganese(II) acetate solution

and TEOS. When TPAOH was added, the solution turned dark brown, indicating the presence of manganese dioxide as a result of oxidation of Mn^{2+} cations in aqueous alkaline medium.^{18,19} The color of the solution remained the same even after 24 h of aging with stirring at room temperature. Because of the facile phase transformation of manganese oxides during synthesis,²⁰ a mixture of manganese oxides (Mn_2O_3 and Mn_3O_4) can be expected. For example, microwave and conventional hydrothermal synthesis under basic conditions can lead to the formation of Mn_3O_4 (from MnO_2),^{21,22} while during calcination (air, 500 °C) decomposition of MnO_2 can occur, producing Mn_2O_3 .²⁰

The maximum crystallization temperature in microwave synthesis was set to 150 °C in order to avoid overheating. Namely, MnO_2 can efficiently absorb microwaves, causing a rapid increase in the temperature and pressure. The advantage of microwave irradiation over the conventional method is in raising the temperature of the whole volume simultaneously, whereas in the heated autoclaves used for conventional hydrothermal synthesis, the reaction solution in contact with the autoclave wall is heated first.¹² In our study, the solution was warmed by microwaves to the desired temperature (150 °C) in a few minutes and the syntheses were completed in 50 min. On the other hand in conventional hydrothermal synthesis, the reaction solution needed several hours to warm up to 175 °C, and the reaction was completed in 24 h. Figure 1 shows XRD patterns of the obtained products after

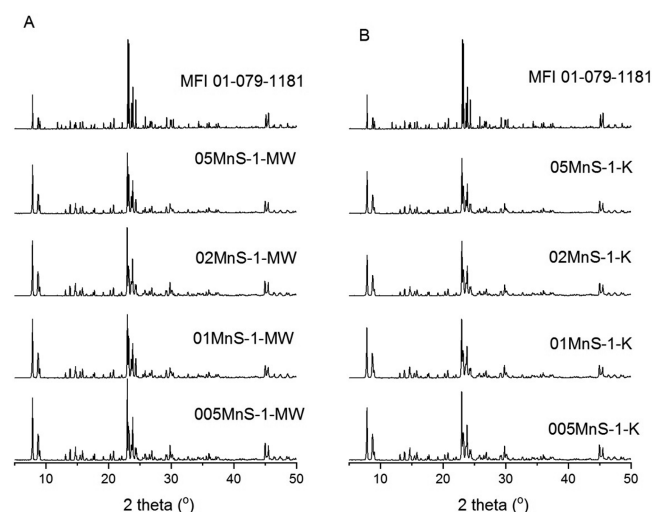


Figure 1. XRD patterns of the MnS-1 nanocrystals, synthesized by (A) a two-step microwave-assisted hydrothermal procedure at 150 °C and (B) a one-step conventional hydrothermal synthesis at 175 °C. 01-079-1181 denotes the reference pattern of MFI topology.

(A) two-step microwave-assisted hydrothermal synthesis and (B) one-step conventional hydrothermal synthesis. All products correspond to the fully crystalline MFI structure with no observable impurities: e.g., manganese oxides. It can be seen that the samples with the highest amount of manganese (05MnS-1) prepared by both synthesis paths show lower intensities of diffraction peaks in comparison to the 005MnS-1 samples.

The manganese content in the investigated samples was determined by EDAX analysis (Table 1). The trend of Mn content within the samples is consistent with the amount of initially added Mn^{2+} precursor.

Table 1. EDX Analysis of All Products Prepared by Microwave and Conventional Synthesis

sample	EDX (wt % of Mn)	Mn/Si
005MnS-1-MW	0.15	0.005
01MnS-1-MW	0.45	0.01
02MnS-1-MW	0.76	0.02
05MnS-1-MW	3.03	0.05
005MnS-1-K	0.38	0.005
01MnS-1-K	0.62	0.01
02MnS-1-K	1.41	0.02
05MnS-1-K	2.78	0.05

The morphology of all products is shown in Figure 2. A comparison of the synthesis method and the morphology of the nanoparticles with the same amount of manganese in the reaction solution ($\text{Mn/Si} = 0.02$) shows spherical shapes formed during conventional heating, while hexagonal prisms were obtained by microwave heating. Size differences can be observed as well: round disks prepared by microwave heating are larger (500 nm) than particles (200 nm) obtained by conventional synthesis from the same reaction solution. Nanocrystals 100–200 nm in size were observed for the first time on comparison to the literature.⁵ A comparison of both synthesis methods points to the advantages of microwave-assisted synthesis for faster growth of crystals in a shorter time. The products (01MnS-1-MW, 02MnS-1-MW, and 05MnS-1-MW) crystallized under microwave heating at 150 °C contain uniform hexagonal prisms (500 nm) and round prisms (005MnS-1-MW) with sizes of 400 nm, depending on the amount of manganese. It can be observed that the morphology and size of the MnS-1-K nanoparticles obtained by the conventional method at 175 °C for 24 h have changed with the amount of the manganese as well, showing 200 nm disk-shaped crystallites with some impurities on the surface of the crystallites when a greater amount of manganese (01MnS-1-MW, 02MnS-1-MW, 05MnS-1-MW) was added to the reaction solution, while a lower amount of manganese ($\text{Mn/Si} = 0.005$) induced the formation of pure 130 nm hexagonal prisms.

The SEM observations in Figure 2A indicate that MnS-1-MW products with lower manganese amounts (0.005 and 0.01) are phase pure, while the product with the highest amount of manganese (0.05) shows the presence of an additional phase in the form of nanorods.

HR-TEM analysis was performed in order to identify the accompanying phase of MnS-1 zeolite crystals. Figure 3a shows typical hexagonal prismatic crystals of silicalite-1 (marked with S) with an estimated size of 500 nm in the 05MnS-1-MW sample. The surfaces of zeolite crystals are covered with nanorods with an average size of 10×50 nm (indicated with Mn on Figure 3a). These nanoparticles exhibit a polycrystalline nature, as indicated by selected area electron diffraction (SAED) performed on the agglomerate shown on Figure 3b. Measured distances of the Scherrer rings on the SAED pattern nicely correspond to hausmannite Mn_3O_4 lattice distances (Figure 3c). A comparison of the measured and referenced d values is also shown in Table 2. An additional confirmation of the hausmannite presence as the extraframework Mn oxide phase in the 05MnS-1 sample was determined by HR-TEM observations on individual rodlike nanocrystals. Figure 3d shows such crystallites oriented on the $[101]$ -zone axis, where

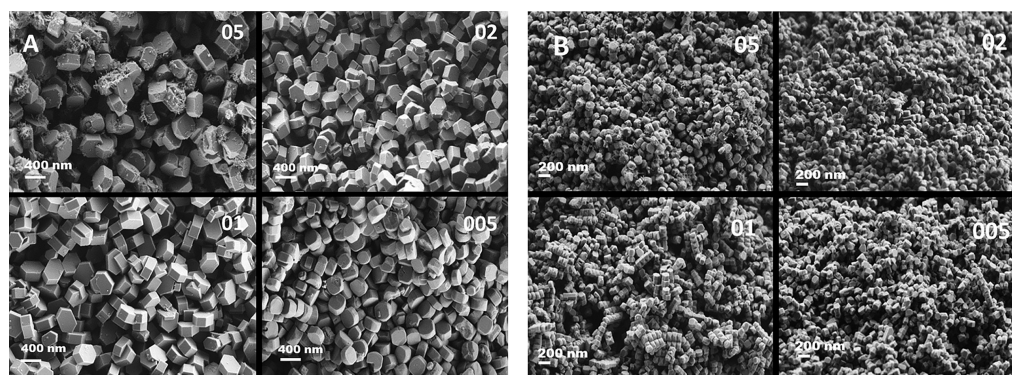


Figure 2. SEM images of the MnS-1 nanocrystals synthesized (A) by a two-step microwave-assisted hydrothermal procedure at 150 °C and (B) by a conventional hydrothermal synthesis at 175 °C.

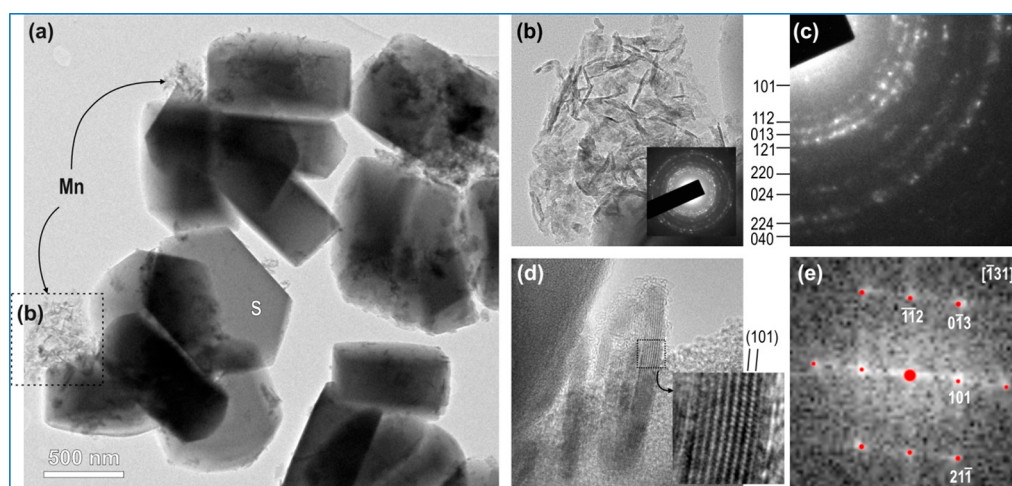


Figure 3. (a) Typical TEM micrograph of 05MnS-1-MW sample. (b) Agglomerate of Mn oxide nanoparticles with the corresponding SAED pattern shown in the inset. (c) Part of the SAED pattern indicating corresponding crystal planes for the Mn_3O_4 (hausmannite) phase. (d) HRTEM image of individual rod-shaped crystallites oriented along the $[101]$ -zone axis as indicated in the inset. (e) FFT pattern performed on the inset area shown in (d) marked with the calculated indices.

Table 2. Comparison of Measured and Referenced d Values of Corresponding Crystal Planes Extracted from SAED Pattern of 05MnS-1-MW Sample

	crystal plane							
	[101]	[112]	[013]	[121]	[220]	[024]	[224]	[040]
measured d value (Å)	5.00	3.18	2.79	2.58	2.08	1.80	1.59	1.26
referenced d value (Å) ^a	4.90	3.09	2.75	2.48	2.03	1.82	1.54	1.23

^aValues are taken from the ICDD database (PDF number 04-004-8640).

reflections of the Fourier transform (FFT) pattern can be unambiguously indexed to the corresponding Mn_3O_4 phase.

On the other hand, TEM observations of the 01MnS-1-MW sample shown in Figure 4 indicate a much lower occurrence of additional Mn oxide species than in the case of the 01MnS-1-MW sample. An additional phase occurs only as individual crystallites on the surface of silicalite crystals (indicated as Mn in Figure 4a), which made their identification by SAED impossible. However, morphological similarity with the rod-shaped crystals that occur in higher concentrations in the 01MnS-1-MW sample clearly identified as Mn_3O_4 (Figure 4b) gives a strong indication that the additional Mn oxide phase in 01MnS-1-MW mostly belongs to the hausmannite phase as well.

However, the presence of both Mn_3O_4 and Mn_2O_3 in the products was expected because of the hydrothermal synthesis performed under basic conditions, necessary to obtain an MFI structure, and calcination in an air flow at 500 °C, respectively. This is in accordance with UV–vis results, which show the presence of the mixture of manganese oxides. Diffuse reflectance UV–vis spectroscopy is used very commonly for the determination of the oxidation and coordination state of metal complexes in solid materials. However, in the case of manganese, the possibility of Mn species with various oxidation states occurring causes difficulties in the interpretation of the experimental results.⁴ UV–vis DR spectra of the samples prepared by microwave and conventional synthesis (Figure 5) are very complex. A band between 253 and 263 nm can be assigned to the framework tetrahedrally coordinated

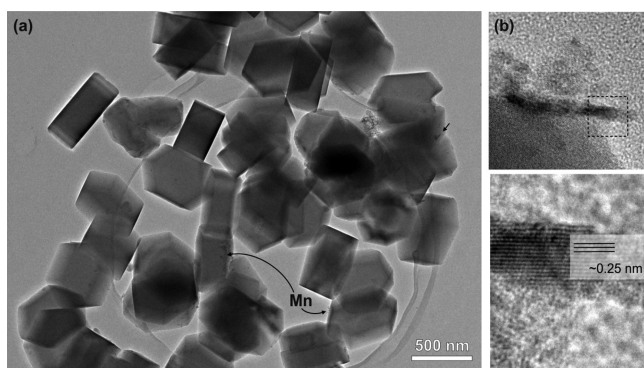


Figure 4. (a) Typical TEM micrograph of the 01MnS-1-MW sample. (b) Individual rod-shaped Mn oxide nanoparticles deposited on the surface of a zeolite crystal. The inset shows an HR-TEM image with the measured interlattice distance.

Mn³⁺.⁵ This band is intense in all samples with Mn/Si higher than 0.01, while for both 005MnS-1 samples it is observed as a shoulder. The broad band around 360 nm with a tail extending to 800 nm, present in 02MnS-1-MW and 05MnS-1-MW, could be due to the extraframework Mn³⁺.^{5,23} The tail extension could indicate also the presence of Mn oxide clusters on the external surface of the zeolite.²⁴ The band (01MnS-1-MW) and shoulder (02MnS-1-MW, 01MnS-1-K, and 02MnS-1-K) around 320 nm indicate the presence of Mn₃O₄.^{25,26} Other bands around 380 and 500 nm due to Mn₂O₃ can be observed.^{23,26} The broad shoulder could indicate the existence of a wide range of distorted-octahedral Mn³⁺ sites that have transitions with a slightly different energy.^{27,28} According to both graphs, higher amounts of manganese (≥ 0.01 MnO) increase the incorporation on framework sites on one side, while on the other side they also promote the formation of oxides. The last trend is especially observed for conventionally prepared samples. Among the samples prepared by microwave heating, the spectra of the 01MnS-1-MW and 05MnS-1-MW show the most intense band at 260 nm, suggesting the largest amount of framework Mn³⁺ in these samples, while this band is even more intense in the samples 01MnS-1-K, 02MnS-1-K, and 05MnS-1-K prepared by conventional synthesis. A more intense broad band at 360 nm can be seen for conventionally prepared samples, indicating that more manganese oxides may be present in these samples. The advantage of microwave-assisted synthesis over conventional synthesis is shown toward

the formation of framework Mn³⁺ when the reaction solution contains 0.01 MnO according to UV–vis spectra.

Although Raman is a sensitive technique which can detect subtle phase information, e.g. framework metal sites in zeolite and extraframework species, it is difficult to resolve between bands due to overlapping. It can be observed that the spectra in Figure 6 can be divided into three main well-resolved peaks. The first peak can be assigned to the characteristic vibrations of the Si–O bonds in the five-membered ring of the MFI structure (372–383 cm⁻¹)^{5,29} and of manganese oxides.³⁰ The second peak, which appears between 550 and 700 cm⁻¹, is typical for Mn–O stretching of octahedral [MnO₆] from manganese oxides,^{30,31} while the last vibrations around 800 cm⁻¹ are characteristic (Si–O–Si or Mn–O–Si) for an MFI structure.⁵ An additional vibration is present around 876 cm⁻¹, which may be assigned to μ -oxo-bridged [Mn₂O]²⁺ species.^{5,32} The most intense vibrations arose from the 05MnS-1-K sample with the highest amount of manganese. Higher amounts of manganese oxides are present in the samples prepared by conventional hydrothermal synthesis, which is in accordance with UV–vis DR spectra. These spectroscopic results reveal Mn²⁺ and Mn³⁺ incorporated in the framework with the coexistence of the manganese oxides placed on the silicalite surface.

Mn K-edge XANES analysis was used to determine the average Mn valence state of Mn cations in the MnS-1 samples with different amounts of Mn from 0.01 to 0.05 Mn/Si, synthesized via a hydrothermal conventional or microwave procedure. No spectra of 005MnS-1-MW or 005MnS-1-K samples were obtained due to the low amount of manganese present in both samples. The normalized XANES spectra of the samples are plotted in Figure 7, together with a selected set of XANES spectra of reference Mn compounds with different Mn valence states and the same manganese ligands (oxygen atoms) as in the investigated samples (Mn²⁺O, Mn^{2.7+}₃O₄, Mn³⁺₂O₃, Mn⁴⁺O₂) and a spectrum of Mn³⁺ cations incorporated into framework positions MnS-1 from our previous studies.³ The valence state of Mn cations in the samples can be deduced from the energy shift of the Mn absorption edge. With increasing oxidation state the Mn absorption edge is shifted to higher energies by about 3.5 eV per unit oxidation state between Mn²⁺ and Mn⁴⁺, as observed for reference Mn compounds (Figure 7) in agreement with previous observations.^{33–35} Mn XANES spectra of all MnS-1 samples exhibit similar (but not identical) Mn K-edge profiles

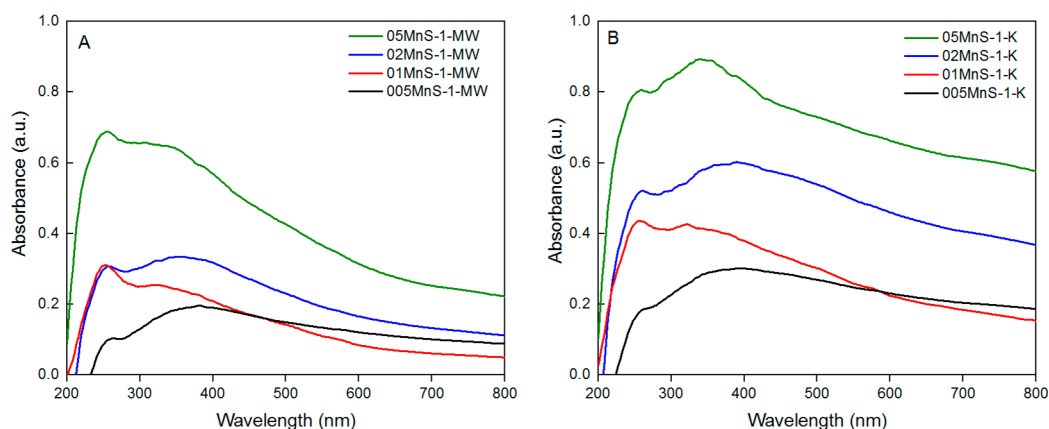


Figure 5. UV–vis DR spectra of (A) MnS-1-MW and (B) MnS-1-K samples.

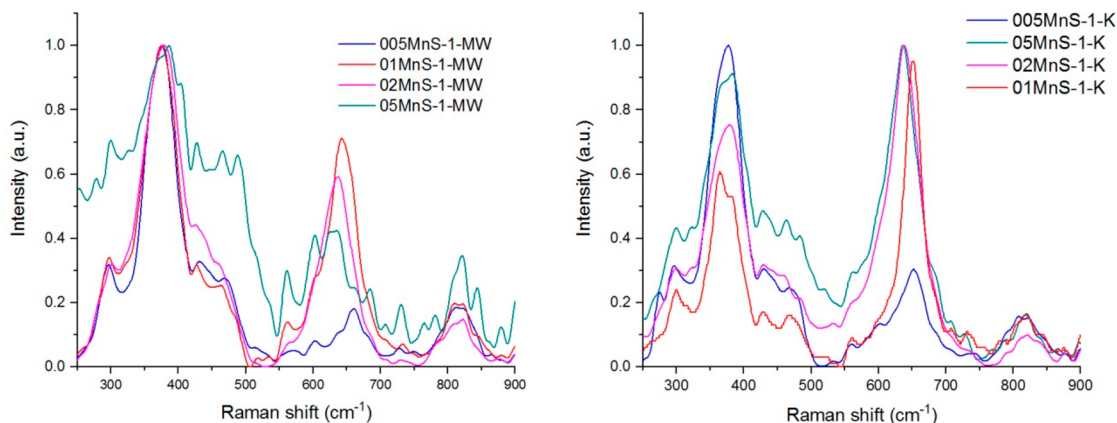


Figure 6. Raman spectra of MnS-1-MW and MnS-1-K samples.

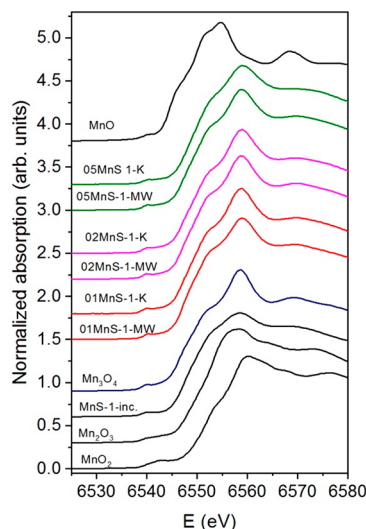


Figure 7. Normalized Mn K-edge XANES spectra of samples MnS-1 synthesized via a hydrothermal conventional or microwave procedure and reference Mn compounds with different Mn valence states and local structures (Mn^{2+}O , $\text{Mn}^{2.7+}_3\text{O}_4$, $\text{Mn}^{3+}_2\text{O}_3$, Mn^{4+}O_2 , and $\text{Mn}^{3+}\text{S1-inc}^3$). The spectra are displaced vertically for clarity.

and energy positions. The edge profiles and positions are close to those of Mn_3O_4 , whose average Mn valence state is 2.7+; therefore, we can deduce that the average Mn valence state in all of the samples is between 2.6+ and 2.8+.

Better insight into the average Mn coordination and chemical state in the MnS-1 samples can be obtained by Mn K-edge EXAFS analysis, which can directly probe the average local structure around Mn cations in the samples. One representative EXAFS spectrum, i.e. the EXAFS spectrum of the 01MnS1-MW sample synthesized via a hydrothermal microwave procedure, was selected for quantitative EXAFS analysis. The Fourier transform magnitude of the EXAFS spectrum (Figure 8) exhibits two dominant peaks in the R range between 1 and 4 Å, representing the contributions of photoelectron scattering on the nearest shells of neighbors around the Mn atom. A strong peak in the R range between 1 and 2.2 Å can be attributed to photoelectron backscattering on the nearest oxygen neighbors around Mn. The following composed peak in the R range between 2.5 and 3.4 Å represents the contributions from more distant Mn coordination shells.

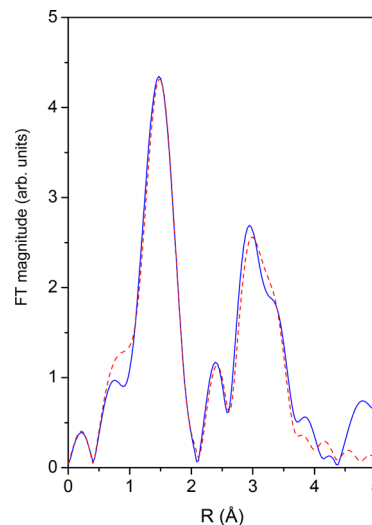


Figure 8. Fourier transform magnitude of the k^3 -weighted Mn EXAFS spectrum of 01MnS-1-MW calculated in the k range of 3.5–12 Å⁻¹ (solid line, experiment; dashed line, best fit EXAFS model).

The EXAFS spectrum was quantitatively analyzed for the coordination number, distance, and Debye–Waller factor of the nearest coordination shells of neighboring atoms. A quantitative analysis was performed with the IFEFFIT program packages¹⁸ using FEFF6 code,¹⁹ in which the photoelectron scattering paths were calculated ab initio from a presumed distribution of neighboring atoms. The atomic species of neighbors are identified in the fit by their specific scattering factor and phase shift. A good fit is obtained in the k range of 3.5–12 Å⁻¹ and an R range from 1 to 4 Å (Figures 8). A complete list of best-fit parameters obtained by EXAFS fit is given in Table 3.

EXAFS analysis shows that manganese cations of the 01MnS-1-MW sample are octahedrally coordinated to six oxygen atoms in the first coordination shell; three of them are at a shorter distance of 1.91 Å, and three of them at a longer distance of 2.27 Å. Mn neighbors are found in the second coordination sphere at the distance of 3.45 Å and oxygen neighbors at 2.9 and 4.1 Å. The obtained structural parameters cannot be assigned to any pure manganese oxide. The EXAFS result indicates that the sample contains a mixture of manganese oxides in the form of nanoparticles or amorphous forms and framework manganese (typically 3-fold coordination

Table 3. Structural Parameters of the Nearest Coordination Shells around Mn Atoms in 01MnS-1-MW: Type of Neighbor Atom, Average Number N , Distance R , and Debye–Waller Factor σ^2 ^a

Mn neighbor	N	R (Å)	σ^2 (Å ²)
O	2.9(6)	1.91(1)	0.006(4)
O	2.8(6)	2.27(1)	0.026(9)
O	2.0(5)	2.94(5)	0.014(5)
Mn	1.1(5)	3.45(5)	0.003(2)
O	4(1)	4.15(5)	0.007(5)

^aThe amplitude reduction factor ($S_0^2 = 0.8$) was determined on MnO and kept fixed during the fit. Uncertainties in the last digit are given in parentheses. The best fit is obtained with the shift of the energy origin $\Delta E_0 = -1.0 \pm 0.6$ eV. The goodness of fit parameter (R factor) is 0.012.

of Mn with O). The average local structure around Mn cations is similar to that found in the case of mesostructured silicate with interparticle porosity Mn/KIL-2 synthesized in our laboratory,³⁶ where Mn cations are present in extraframework manganese oxide nanoparticles with typical dimensions of 2 nm, homogeneously distributed throughout the material.

Small structural differences of other MnS-1 samples in comparison to the 01MnS1-MW sample can be deduced by a comparison of their XANES spectra. Linear combination fits of XANES spectra show that spectra of all other MnS-1 samples can be described as a linear combination of the spectrum of the 01MnS1-MW sample as a dominant component and small amounts of XANES spectra of three reference Mn oxides ($\text{Mn}^{2.7+}_3\text{O}_4$, $\text{Mn}^{3+}_2\text{O}_3$, Mn^{4+}O_2) (Figure 9). Thus, we can conclude that all MnS-1 spectra are composed of slightly different mixtures of manganese oxides, most probably in the form of nanoparticles or amorphous forms.

Catalytic Performance. Catalytic styrene epoxidation was performed over MnS-1-MW and MnS-1-K samples with

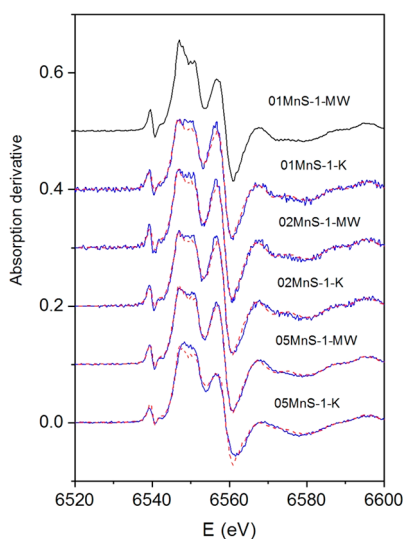


Figure 9. Derivatives of normalized Mn K-edge XANES spectra of all samples MnS-1 with different amounts of MnO from 0.01 to 0.05, synthesized via a hydrothermal conventional or microwave procedure (solid line, experiment; dashed line, linear combination fit with XANES spectra of the spectrum of 01MnS1-MW and spectra of three reference Mn oxides (Mn_3O_4 , Mn_2O_3 , MnO_2)). The spectra are displaced vertically for clarity.

different Mn/Si molar ratios of 0.005, 0.01, 0.02, and 0.05. Figure 10 shows the conversion of styrene after 24 h for

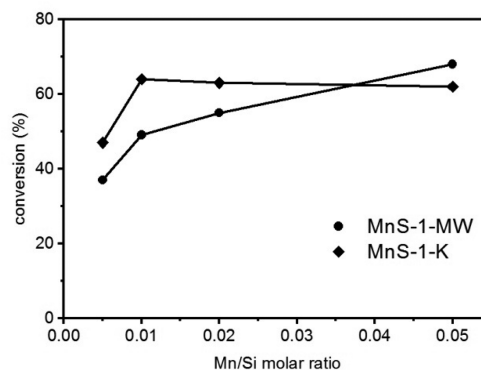


Figure 10. Conversion of styrene after 24 h for MnS-1-MW and MnS-1-K with different Mn/Si molar ratios.

materials prepared by microwave-assisted synthesis (MnS-1-MW) and a conventional hydrothermal method (MnS-1-K) with different Mn/Si molar ratios.

For MnS-1-K samples with Mn/Si molar ratios 0.01, 0.02, and 0.05 essentially the same conversion after 24 h reaction time was observed. Evidently, the conversion of styrene is independent of the Mn/Si molar ratio and there is no difference between MnS-1 containing framework Mn^{3+} and the extraframework Mn^{3+} . In contrast, the conversion over the materials obtained by microwave-assisted synthesis increases with increasing Mn/Si molar ratio. Over the material with Mn/Si = 0.05, the conversion is even higher than that over the material from the conventional hydrothermal synthesis. In other words, the materials from conventional hydrothermal synthesis and with Mn/Si ≤ 0.02 are catalytically more active than the materials from microwave-assisted synthesis with the same Mn/Si molar ratio, possibly due to the lower size of the crystals and different molar ratio of Mn-containing species. Figure 11 shows the initial reaction rates of the styrene

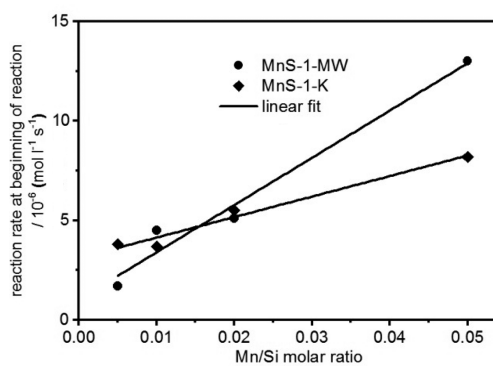


Figure 11. Reaction rate at the beginning of styrene epoxidation over MnS-1-MW and MnS-1-K with different Mn/Si molar ratios.

epoxidation over the MnS-1-MW and MnS-1-K materials with different Mn/Si molar ratios, respectively. For both materials, the initial reaction rate increases with increasing Mn/Si molar ratio as expected. However, the increase for the MnS-1-MW materials is more pronounced than for the MnS-1-K materials.

CONCLUSIONS

In summary, Mn^{3+} species can be placed into zeolite silicalite-1 with MFI structure by microwave heating at 150 °C in less than 1 h and by conventional hydrothermal synthesis at a higher crystallization temperature of 175 °C and longer crystallization time of 24 h. Nanosized crystals with a size of 200 nm were obtained from reaction solutions having the composition 10 SiO_2 :0.02–0.05 MnO :4 TPAOH:195 H_2O by a conventional procedure and 500 nm by a microwave procedure, while even smaller nanoparticles were obtained from reaction mixtures with lower Mn/Si in both procedures. The amount of manganese influences the morphology and the size of nanocrystals as well as the formation of manganese oxides on the external surface of the particles. The analyses of UV–vis and Raman spectra of all samples proved the incorporation of Mn^{3+} into the framework and the formation of manganese oxides (Mn_2O_3 and Mn_3O_4). TEM and XAS spectroscopy showed the presence of Mn_3O_4 . Thus, the incorporation of Mn species can be tuned by the amount of manganese in the reaction solution and the choice of preparation procedure. In addition, MnS-1-MW and MnS-1-K with different Mn/Si molar ratios of 0.005, 0.01, 0.02, and 0.05 were studied as catalysts in the epoxidation of styrene. The materials from conventional hydrothermal synthesis and with $Mn/Si \leq 0.02$ are catalytically more active than the materials from microwave-assisted synthesis with the same Mn/Si molar ratio, possibly due to the lower size of the crystals and different molar ratio of Mn-containing species.

AUTHOR INFORMATION

Corresponding Author

*N.N.T.: tel, +386 1 4760410; fax: 386 1 4760300; e-mail, natasa.novak.tusar@ki.si.

ORCID

Matjaž Mazaj: 0000-0003-3196-9079

Nataša Novak Tušar: 0000-0001-7098-2255

Notes

The authors declare no competing financial interest.

ACKNOWLEDGMENTS

This research was supported by the Slovenian Research Agency through research programs P1-0021 and P1-0112 and partially by the project CALIPSOplus under the Grant Agreement 730872 from the EU Framework Programme for Research and Innovation HORIZON 2020. Access to the synchrotron radiation facilities of DESY, a member of the Helmholtz Association (HGF) (beamline P65 pr. I-20170160 EC), and ELETTRA (beamline XAFS, project 20165258) is acknowledged. We thank Edmund Welter of HASYLAB and Clara Guglieri Rodriguez, Giuliana Aquilanti, and Luca Olivi of ELETTRA for expert advice on beamline operation, Dr. Petar Djinović for UV–vis measurements, and Mojca Opresnik for SEM microscopy.

REFERENCES

- (1) Novak Tušar, N.; Jank, S.; Gläser, R. Manganese-Containing Porous Silicates: Synthesis, Structural Properties and Catalytic Applications. *ChemCatChem* **2011**, *3*, 254–269.
- (2) Kosinov, N.; Liu, C.; Hensen, E. J. M.; Pidko, E. A. Engineering of Transition Metal Catalysts Confined in Zeolites. *Chem. Mater.* **2018**, *30*, 3177–3198.

- (3) Tušar, N. N.; Logar, N. Z.; Arčon, I.; Thibault-Starzyk, F.; Ristić, A.; Rajić, N.; Kaučič, V. Manganese-Containing Silica-Based Microporous Molecular Sieve MnS-1: Synthesis and Characterization. *Chem. Mater.* **2003**, *15*, 4745–4750.

- (4) Baran, R.; Valentin, L.; Dzwigaj, S. Incorporation of Mn into the Vacant T-Atom Sites of a BEA Zeolite as Isolated, Mononuclear Mn: FTIR, XPS, EPR and DR UV-Vis Studies. *Phys. Chem. Chem. Phys.* **2016**, *18*, 12050–12057.

- (5) Meng, Y.; Genuino, H. C.; Kuo, C.-H.; Huang, H.; Chen, S.-Y.; Zhang, L.; Rossi, A.; Suib, S. L. One-Step Hydrothermal Synthesis of Manganese-Containing MFI-Type Zeolite, Mn-ZSM-5, Characterization, and Catalytic Oxidation of Hydrocarbons. *J. Am. Chem. Soc.* **2013**, *135*, 8594–8605.

- (6) Zhao, J.; Zhang, Y.; Zhang, S.; Wang, Q.; Chen, M.; Hu, T.; Meng, C. Microporous and Mesoporous Materials Synthesis and Characterization of Mn-Silicalite-1 by the Hydrothermal Conversion of Mn-Magadiite under the Neutral Condition and Its Catalytic Performance on Selective Oxidation of Styrene. *Microporous Mesoporous Mater.* **2018**, *268*, 16–24.

- (7) Iida, T.; Kohara, S.; Okubo, T.; Numako, C.; Nakahira, A.; Sato, M.; Wakihara, T. Preparation and Characterization of Silicalite-1 Zeolites with High Manganese Contents from Mechanochemically Pretreated Reactants. *J. Mater. Chem. A* **2015**, *3*, 6215–6222.

- (8) Mintova, S.; Jaber, M.; Valtchev, V. Nanosized Microporous Crystals: Emerging Applications. *Chem. Soc. Rev.* **2015**, *44*, 7207–7233.

- (9) Lupulescu, A. I.; Rimer, J. D. Supplementary Materials for In Situ Imaging of Silicalite-1 Surface Growth Reveals the Mechanism of Crystallization Movies S1 and S2. *Science (Washington, DC, U. S.)* **2014**, *344*, 729–733.

- (10) Meng, X.; Xiao, F. S. Green Routes for Synthesis of Zeolites. *Chem. Rev.* **2014**, *114*, 1521–1543.

- (11) Whittaker, A. G.; Carassiti, L.; Tapia-Ruiz, N.; Kitchen, H. J.; Harrison, A.; Kennedy, J. L.; Kingman, S. W.; Vallance, S. R.; Gregory, D. H.; Drysdale, T. D. Modern Microwave Methods in Solid-State Inorganic Materials Chemistry: From Fundamentals to Manufacturing. *Chem. Rev.* **2014**, *114*, 1170–1206.

- (12) Zhu, Y.; Chen, F. Microwave-Assisted Preparation of Inorganic Nanostructures in Liquid Phase. *Chem. Rev.* **2014**, *114*, 6462–6555.

- (13) Tušar, N. N.; Mauček, D.; Rangus, M.; Arčon, I.; Mazaj, M.; Cotman, M.; Pintar, A.; Kaučič, V. Manganese Functionalized Silicate Nanoparticles as a Fenton-Type Catalyst for Water Purification by Advanced Oxidation Processes (AOP). *Adv. Funct. Mater.* **2012**, *22*, 820–826.

- (14) Lapornik, V.; Novak Tusar, N.; Ristic, A.; Chellappan, R. K.; Foix, D.; Dedryvère, R.; Gaberscek, M.; Dominko, R. Manganese Modified Zeolite Silicalite-1 as Polysulphide Sorbent in Lithium Sulphur Batteries. *J. Power Sources* **2015**, *274*, 1239–1248.

- (15) Ravel, B.; Newville, M. ATHENA, ARTEMIS, HEPHAESTUS: Data Analysis for X-Ray Absorption Spectroscopy Using IFEFFIT. *J. Synchrotron Radiat.* **2005**, *12*, 537–541.

- (16) Rehr, J. J.; Albers, R. C.; Zabinsky, S. I. High-Order Multiple-Scattering Calculations of x-Ray-Absorption Fine Structure. *Phys. Rev. Lett.* **1992**, *69*, 3397–3400.

- (17) Ramanathan, A.; Archipov, T.; Maheswari, R.; Hanefeld, U.; Roduner, E.; Gläser, R. Synthesis, Characterization and Catalytic Properties of the Novel Manganese-Containing Amorphous Mesoporous Material MnTUD-1. *J. Phys. Chem. C* **2008**, *112*, 7468–7476.

- (18) Boumaiza, H.; Coustel, R.; Medjahdi, G.; Ruby, C.; Bergaoui, L. Conditions for the Formation of Pure Birnessite during the Oxidation of Mn(II) Cations in Aqueous Alkaline Medium. *J. Solid State Chem.* **2017**, *248*, 18–25.

- (19) Balan, L.; Matei Ghimbeu, C.; Vidal, L.; Vix-Guterl, C. Photoassisted Synthesis of Manganese Oxide Nanostructures Using Visible Light at Room Temperature. *Green Chem.* **2013**, *15*, 2191–2199.

- (20) Han, Y.-F.; Chen, F.; Zhong, Z.; Ramesh, K.; Chen, L.; Widjaja, E. Controlled Synthesis, Characterization, and Catalytic Properties of

Mn₂O₃ and Mn₃O₄ Nanoparticles Supported on Mesoporous Silica SBA-15. *J. Phys. Chem. B* **2006**, *110*, 24450–24456.

(21) Lee, J. W.; Hall, A. S.; Kim, J.-D.; Mallouk, T. E. A Facile and Template-Free Hydrothermal Synthesis of Mn₃O₄ Nanorods on Graphene Sheets for Supercapacitor Electrodes with Long Cycle Stability. *Chem. Mater.* **2012**, *24*, 1158–1164.

(22) Yang, L.-X.; Zhu, Y.-J.; Tong, H.; Wang, W.-W.; Cheng, G.-F. Low Temperature Synthesis of Mn₃O₄ Polyhedral Nanocrystals and Magnetic Study. *J. Solid State Chem.* **2006**, *179*, 1225–1229.

(23) Tang, Q.; Hu, S.; Chen, Y.; Guo, Z.; Hu, Y.; Chen, Y.; Yang, Y. Highly Dispersed Manganese Oxide Catalysts Grafted on SBA-15: Synthesis, Characterization and Catalytic Application in Trans-Stilbene Epoxidation. *Microporous Mesoporous Mater.* **2010**, *132*, 501–509.

(24) Zhou, W.-F.; Chen, L.; Xie, J.; Au, C.-T.; Yin, S.-F. Efficient Synthesis of p-Chlorobenzaldehyde through Liquid-Phase Oxidation of p-Chlorotoluene Using Manganese-Containing ZSM-5 as Catalyst. *RSC Adv.* **2015**, *5* (91), 74162–74169.

(25) Kumar, A.; Nepak, D.; Srinivas, D. Direct Synthesis of Amides from Amines Using Mesoporous Mn-SBA-12 and Mn-SBA-16 Catalysts. *Catal. Commun.* **2013**, *37*, 36–40.

(26) Velu, S.; Shah, N.; Jyothi, T. M.; Sivasanker, S. Effect of Manganese Substitution on the Physicochemical Properties and Catalytic Toluene Oxidation Activities of Mg–Al Layered Double Hydroxides. *Microporous Mesoporous Mater.* **1999**, *33*, 61–75.

(27) Radu, D.; Glatzel, P.; Gloter, A.; Stephan, O.; Weckhuysen, B. M.; de Groot, F. M. F. Geometric and Electronic Structure of α -Oxygen Sites in Mn-ZSM-5 Zeolites. *J. Phys. Chem. C* **2008**, *112*, 12409–12416.

(28) Klokishner, S. I.; Reu, O.; Chan-Thaw, C. E.; Jentoft, F. C.; Schlögl, R. Redox Properties of Manganese-Containing Zirconia Solid Solution Catalysts Analyzed by In Situ UV–Vis Spectroscopy and Crystal Field Theory. *J. Phys. Chem. A* **2011**, *115*, 8100–8112.

(29) Lita, A.; Ma, X.; Meulenberg, R. W.; van Buuren, T.; Stigman, A. E. Synthesis and Characterization of Phase-Pure Manganese(II) and Manganese(III) Silicalite-2. *Inorg. Chem.* **2008**, *47*, 7302–7308.

(30) Julien, C.; Massot, M.; Poinson, C. Lattice Vibrations of Manganese Oxides. *Spectrochim. Acta, Part A* **2004**, *60*, 689–700.

(31) Sun, M.; Lan, B.; Yu, L.; Ye, F.; Song, W.; He, J.; Diao, G.; Zheng, Y. Manganese Oxides with Different Crystalline Structures: Facile Hydrothermal Synthesis and Catalytic Activities. *Mater. Lett.* **2012**, *86*, 18–20.

(32) Smeets, P. J.; Woertink, J. S.; Sels, B. F.; Solomon, E. I.; Schoonheydt, R. A. Transition-Metal Ions in Zeolites: Coordination and Activation of Oxygen. *Inorg. Chem.* **2010**, *49*, 3573–3583.

(33) Ressler, T.; Wong, J.; Roos, J. Manganese Speciation in Exhaust Particulates of Automobiles Using MMT-Containing Gasoline. *J. Synchrotron Radiat.* **1999**, *6*, 656–658.

(34) Arcon, I.; Hanzel, D.; Dominko, R.; Masquelier, C.; Gaberscek, M.; Sirisopanaporn, C. On the Origin of the Electrochemical Capacity of Li₂Fe_{0.8}Mn_{0.2}SiO₄. *J. Electrochem. Soc.* **2010**, *157*, A1309.

(35) Tušar, N. N.; Logar, N. Z.; Vlačić, G.; Arčon, I.; Arčon, D.; Daneu, N.; Kaučič, V. Local Environment of Manganese Incorporated in Mesoporous MCM-41. *Microporous Mesoporous Mater.* **2005**, *82*, 129–136.

(36) Tušar, N. N.; Ristić, A.; Mali, G.; Mazaj, M.; Arčon, I.; Arčon, D.; Kaučič, V.; Logar, N. Z. MnO Nanoparticles Supported on a New Mesostructured Silicate with Textural Porosity. *Chem.-Eur. J.* **2010**, *16*, 5783–5793.